Hindawi
Journal of Sensors
Volume 2020, Article ID 8847114, 13 pages
https://doi.org/10.1155/2020/8847114

Research Article

Determination of Glycaemic Index (GI) through Detecting Insulin Secretion in Pancreas Using GMR Sensor

P. Sankari,[1] **N. Prabavathi**,[2] **and N. R. Shanker**[3]

[1]*Government Arts College for Women, Salem-8, India*
[2]*Sri Sarada College for Women, Salem-16, India*
[3]*Aalim Muhammed Salegh College of Engineering, Chennai-55, India*

Correspondence should be addressed to P. Sankari; sankaripkg@gmail.com

Received 16 April 2020; Revised 2 July 2020; Accepted 28 August 2020; Published 18 September 2020

Academic Editor: Gwanggil Jeon

Diabetes is a metabolic disease that affects the ability of the body to process blood glucose, otherwise known as blood sugar. Diabetes occurs when the body produces minimal or no insulin. The diabetes patients check their glycaemic index after each meal and intake medicine to control glycaemic index. Traditionally, glycaemic index estimates the glucometer by acquiring blood sample. In this paper, we propose a noninvasive method to estimate glycaemic index from the pancreas. The magnetic signal from the pancreas acquires with Giant Magneto Resistance (GMR) sensor for glycaemic index estimation. The GMR acquired pancreatic magnetic signal process with Multi Synchro Squeezing Transform (MSST) for feature extraction. The MSST analysis shows significant changes in instantaneous frequency of the pancreas biomagnetic signal before and after meal consumption. The signal statistical parameters help to predict glycaemic index via regression modelling. The proposed method estimates glycaemic index with 88% accuracy.

1. Introduction

The autoimmune diseases are caused due to the effect of self-immune system detecting its own proteins as antigens and perform an attack over its own tissues. These are caused due to the genetic proneness over the stimulus of prior environmental disease commencement. Blood glucose is the main source of energy and comes from the food. Insulin, a hormone made by the pancreas, helps glucose from food get into the cells to be used for energy. All carbohydrate foods are broken down into glucose in the blood. Insulin helps glucose get into the cells. Hyperglycaemia is a condition, where the body cannot produce insulin or use it which effectively leads to raised glucose levels. High glucose levels over the long term will cause damage to the body and failure of various organs and tissues [1]. Diabetes is a chronic disease caused due to the swelling of T-cells, which causes autoimmune disorder that destroys the β-cells in the pancreas. These are the base cells for producing insulin for regulating the blood glucose level.

This develops the impairment in maintaining glucose level in the blood. The insulin helps the cells to consume glucose from the blood stream. Nearly 70 to 80% of β-cells are present in the islet of the pancreas and it covers 1 to 2% of the pancreas total size. The islet is covered by glucagon, somatostatin, and pancreatic polypeptide. These are responsible for generation of α-cells, δ-cells, and ε-cells. The pancreas acts as a digestive organ that generates lytic enzymes for the catabolism of nutrients.

Type 1 diabetes can develop at any age, but occurs frequently in children and adolescents. People with type 1 diabetes need daily insulin injections to control their blood glucose levels. If people with type 1 diabetes do not have access to insulin, they will die. The risk factors for type 1 diabetes are still under research. A family member with type 1 diabetes slightly increases the risk of developing the disease. At present, type 1 diabetes cannot be prevented. The environmental triggers that are thought to generate the process that results in the destruction of the body's insulin-producing cells are still under investigation. The most common

symptoms of type 1 diabetes include abnormal thirst and dry mouth, sudden weight loss, frequent urination, lack of energy, tiredness, constant hunger, blurred vision, and bedwetting.

Type 2 diabetes is more common in adults and accounts for around 90% of all diabetes cases. In type 2 diabetes, the body does not make good use of the insulin that it produces. It is generally characterized by insulin.

The insulin secretion activity happens in the pancreas. Therefore, diabetes can be detected through analyzing the functioning of pancreas. It has a flat pear-like shape and is surrounded by the stomach, small intestine, liver, spleen, and gallbladder. The pancreas's wide end on the body's right side is called the head. The middle sections are the neck and body. The thin end of the pancreas on the left side of the body is called the tail. The uncinate process happens in the pancreas that bends backwards and underneath the head of the pancreas. Two significant blood vessels, the superior mesenteric vein and superior mesenteric artery, cross behind the neck of the pancreas and in front of the uncinate process. The pancreas is both an exocrine gland and endocrine gland and has two main functions—digestion and blood sugar regulation.

Exocrine cells of the pancreas produce enzymes that help with digestion. When food enters the stomach, exocrine cells release the pancreatic enzymes into a system of small ducts that lead to the main pancreatic duct. The pancreatic duct runs the length of the pancreas and carries pancreatic enzymes and other secretions, collectively called pancreatic juice. The main pancreatic duct connects with the common bile duct, which carries bile from the gallbladder, and together, they connect with the duodenum at a point called the ampulla of Vater. Here, bile and pancreatic enzymes enter the duodenum to aid with the digestion of fats, carbohydrates, and proteins [2]. The blood glycaemic index (GI) measures the glucometer after consuming food to know the food's insulin response in the pancreas. In this paper, we propose a noninvasive way to measure glycaemic index based on the pancreas biomagnetic emission. The biomagnetic emission measures with the GMR sensor. The GMR sensor has an excellent magnetic linear sensitivity of 98% and produces a ratiometric output. The GMR sensor has been tested for implantable medical applications.

2. Literature Survey

Continuous glucose monitoring (CGM) devices are based on microelectromechanical systems, which show capacitivity. The sensor consists of a vibrating Parylene diaphragm, which is remotely driven by a magnetic field and situated inside a microchamber. A solution of poly(acrylamide-ran-3-acrylamidophenylboronic acid) (PAA-ran-PAAPBA), a biocompatible glucose-sensitive polymer, fills the microchamber, which is separated from its surroundings by a semipermeable membrane. Glucose permeates through the membrane and binds reversibly to the phenylboronic acid moiety of the polymer. This results in a viscosity change of the sensing solution, causing a detectable change in the Parylene diaphragm vibration which can be measured capacitively [1].

A new smart phone-based reusable glucose meter includes a custom-built smart phone case that houses a permanent bare sensor strip, a stylus that is loaded with enzyme-carbon composite pellets and sensor instrumentation circuits. A custom-designed android-based software application was developed to enable easy and clear display of measured glucose concentration. A typical test involves the user loading the software using the stylus to dispense an enzymatic pellet on top of the bare sensor strip affixed to the case and then introducing the sample. The electronic module then acquires and wirelessly transmits the data to the application software to be displayed on the screen. The deployed pellet is then discarded to regain the fresh bare sensor surface. Such a unique working principle allows the system to overcome challenges by previously reported reusable sensors, such as enzyme degradation, leaching, and hysteresis effects. The enzymes loaded in the pellets are stable for up to 8 months at ambient conditions and generate reproducible sensor signals. The significance of the pellet-based sensing system towards reusable, point-of-care sensor is that it fits closely around smart phone and does not face issues usually common to reusable sensors. The versatility of this system allows it to be easily modified to detect other analytes for application in a wide range of healthcare, environmental, and defense domains [3].

The availability of new minimally invading subcutaneous sensors for monitoring glucose level continuously researches on a new online for improving the treatment of diabetes, including hyper/hypoglycaemic alert generators and artificial pancreas. Continuous glucose monitoring (CGM) signals affect with the random measurement noise with these applications is an important aspect to be taken. The major difficulty is that for a given sensor technology, the signal-to-noise ratio (SNR) can vary from subject to subject (interindividual variability) and also within subject (intraindividual variability). A Kalman filter is implemented with parameters automatically tuned, for one time, in a burn-in interval with the interindividual variability of SNR. This method resorts to a Bayesian smoothing procedure that uses a statistically based criterion for a continuous update, to determine filter parameters in real time. CGM signals are noisy and it is crucial to improve their quality [4].

Diabetes is a serious problem that can only be delayed or prevented by a regular monitoring of blood glucose (BG) concentration level. Continuous glucose monitoring system allows preparing diabetes management strategy and preventing the long-term complication diseases. Here, a new BG sensor is introduced which is cost-efficient and highly wearable with a small data acquisition time window that allows a noninvasive, long-term continuous blood glucose monitoring (CGM) system. The biosensor efforts a unique information beaten to continuous components of the arterial blood volume pulsation during the change of blood glucose (BG) concentration at the wrist tissue. Near infrared (Vis-NIR) spectroscopy is measured in the combine reflected optical signal [5].

Diabetes is a widespread disease over 285 million cases approximately. The miniaturized sensor was kept under the eyelid. The sensor consists of an ASIC set with integrated

potentiostat and chrono-amperometric glucose and transponder circuits. ISO 18000-3 is the passive transponder which is used to power and read out the sensor for the wireless energy and data transmission. A combination of antenna and sensor electrode wires is attached for high integration level [6].

A system incorporates a control algorithm with pumps to automate the delivery of the hormones glucagon and with off-the-shelf subcutaneous sensors and insulin with respect to continuous glucose sensor measurements. Proportional derivative control algorithm decides hormone delivery rates that are based on the sensed glucose measurements and the meal announcements by the patient for the automated component of the system. The system design and the control algorithm are provided for both the fading memory proportional derivative controller (FMPD) and the adaptive system which is based on a glucoregulatory model of insulin action for determining the changes of insulin sensitivity [7].

Diabetic is the rate of acetone changes in the human breath. Different gases are produced in the organs of the human body. The breath passes through the alveoli when it is transmitted to the lungs and into the blood gases during the cleaning of the blood. Human breath acetone concentration is very low (0.1-10 ppm). The finding of the human blood glucose and HbA1c levels from exhaled breath is based on quartz crystal microbalance (QCM) sensors with the help of an electronic nose system. The amount of acetone vapour, which is the marker of blood glucose, is 0.1-10 ppm in human expiration. Radial basis function neural network (RBFNN) is compared against glucose and HbA1c parameters which is used in electronic nose of the data of the QCM sensor [8].

In diabetes management, glucose concentration is an important task for the prevention of hypo/hyperglycaemic events. Continuous glucose monitoring (CGM) devices predict glucose of the body by monitoring every 3 minutes and using a first-order polynomial or a first-order autoregressive (AR) model, both with time-varying parameters determined by weighted least squares are described of past glucose data. By using this methods, glucose can be predicted ahead in time, e.g., with a prediction of 30 min crossing of the hypoglycaemic threshold which can be predicted by 20-25 min ahead in time, with the sufficient margin to the event by sugar ingestion [9].

Some dogs also form the diabetes mellitus similar to that seen in children. It is mainly concurrent by high blood glucose (BG) and urine concentrations. Breath acetone analysis concentrations are elevated and observed that the correlation between breath acetone and BG has to be determined in type 1 DM in humans. Breath acetone in diabetic dogs might allow the use of breath acetone as a biomarker for diabetes in both humans and animals [10].

Ni–$SnO_{x,}$ PANI, and CuO nanoparticles are used to make a new elastic high-performance nonenzymatic glucose sensor that was synthesized on cotton fabric through chemical methods. A conductive template made of nickel and copper oxide and hydroxide with the high electrochemical performance with an electrocatalytic activity oxidize glucose excellently which leads to fabrication of a wearable and flexible cotton electrode [11].

Microfabricated and micropatterned on a flexible polyimide substrate uses a reduced graphene oxide- (rGO-) based nanostructured composite working electrode of high quality. To develop a human sweat-based wearable glucose sensor application, gold and platinum alloy nanoparticles were electrochemically deposited onto the microfabricated rGO surface and chitosan-glucose oxidase composites were incorporated onto the modified surface of the working electrode. An amperometric response to glucose in the fabricated biosensor has a detection range of 0-2.4 mM (covers the glucose range in sweat), with a short response time (20 sec), with a sensitivity of $48\,\mu A/mM\,cm^2$, and high linearity (0.99). The detection limit for glucose is found to be $5\,\mu m$. Testing the acceptable detection performance and stability for low glucose concentrations initially occurs when the human sweat/mixing glucose samples occurs. The results from the nanostructured composite flexible working electrode and fabrication process for application as human sweat-based electrochemical glucose sensors performed well [12].

Through the ultraviolet mediated chemical plating technique, a thin film PET based gold electrode (PGE) glucose sensor is fabricated. The PGE-glucose sensor is simple and low cost, and minimum instrumentation is required when compared with the most of the existing wearable thin film gold electrode sensors. In the previous, glucose sensor discloses a sensitivity of $22.05\,A/mM^{-1}\,cm^{-2}$ in a linear range from 0.02 to 1.11 mM with a low detection limit of $2.7\,\mu m$ ($S/N = 3$). The PGE-glucose sensor has a good selectivity and not steps in by lactic acid, urea, acetaminophene, uric acid, dopamine, and ascorbic acid. In addition to that, it exhibits good reproducibility and long-term stability over four weeks [13].

Glassy carbon electrode (GCE) with graphene oxide (GO), NiO nanofibers (NiONFs), and Nafion (NA) modify a glucose sensor. Electrospinning technique followed by calcination was done to produce NIONFs and GO that was synthesized by Hummers' method. The modified electrode was pretreated by the electrochemical reduction. The sensor characterization was carried out with scanning electron microscopy (SEM), energy dispersive X-ray spectroscopy (EDX), X-ray photoelectron spectroscopy (XPS), and electrochemical impedance spectroscopy (EIS). The sensor shows high sensitivity ($1100\,\mu A/mM^{-1}\,cm^{-2}$), fast response time (less than 5 s), low detection limit of $0.77\,\mu m$ (S/N-3), long-term stability, and excellent antifouling ability for glucose determination. Here, GO is reduced by electrochemical method, which is simple, efficient, low cost, and environmental friendly [14].

The major insulin-secreting pancreatic β-cells are destroyed when diabetes is diagnosed. The β-cell is destroyed over many years, making timely detection and clinical intervention difficult. There is vast interest in developing tools to bioimage β-cell mass to function noninvasively to facilitate early diagnosis of diabetes in order to assist the development of novel antidiabetic therapies. The need of human β-cells is to bioimage noninvasively in various types of diabetes by current and emerging tools for bioimaging β-cells [15].

Type 1 diabetes is an autoimmune disease by immune cells that selectively kill the β-cells or pancreatic islets. The rodent and human T lymphocytes release exosomes containing the microRNAs (miRNAs) miR-142-3p, miR-142-5p, and miR-155 and were transferred in active form to β-cell favoring apoptosis. Islets from protected NOD mice display higher insulin levels, lower insulin scores, and reduced inflammation. The mechanism in some action found that T lymphocyte exosomes trigger apoptosis and the expression of genes involved in chemokine signaling, including Cc/2, Cc/7, and Cxc/10 exclusively in β-cells. The recruitment of immune cells and exacerbate β-cell death can have induction of these genes during the autoimmune attack [16].

The glaucoma disease diagnose at early stage with biomagnetic signal of aqueous humor fluid present in anterior chamber of eye. The aqueous fluid emits magnetism due to its composition such as sodium, chloride, potassium, and protein. The GMR detects biomagnetic signal from aqueous humor of eye. The biomagnetic signal variation is analyzed with the rational dilation wavelet transform for static and dynamic nature of aqueous humor fluid [17].

3. Methodology

The Figure 1 shows the proposed method workflow to determine the magnetic signal emission from the pancreas. The GMR sensor is placed over the pancreas region as shown in Figure 2. The GMR sensor detects magnetic emission from the pancreas and produces proportional voltage signal. The GMR output signal acquires and saves with data acquisition tool. The signal acquires for two cases. The GMR signal acquires for case 1 (before meal consumption) and case 2 (after meal consumption). The signal analyzes with MSST to differentiate changes in magnetic signal due to meal consumption. The statistical parameters extract from biomagnetic signal for glycaemic index prediction. The predicted values are compared with traditional glucometer values.

3.1. GMR Sensor. The Giant Magneto Resistance undergoes change in electrical resistance in response to a change in applied magnetic field. The GMR sensor works based on quantum mechanical effect. The effect is caused due to spin-dependent scattering process in magnetic multilayers of GMR sensor. The resistance changes in the multilayer when the external magnetic field aligns the successive ferromagnetic layers' magnetic moments. When the magnetic field is not present, the magnetic layers' magnetic moments are aligned with respect to each other and the resistance increases. The resistance decreases only when the magnetic moments of ferromagnetic layers are aligned by the applied magnetic field.

3.2. Multi Synchro Squeezing Transform (MSST). The acquired magnetic signal processes with Multi Synchro Squeezing Transform (MSST). Time frequency analysis (TFA) is an essential tool for analyzing time-varying oscillatory signals. The classical techniques such as short-time Fourier transform and wavelet transform expand a one-dimensional time-series signal into two-dimensional time frequency plane. From the TF plane, several time-varying features can be observed and signal decomposition can be performed easily. Due to Heisenberg's uncertainty principle, conventional techniques yielding TF representations are not clear and it is not possible to describe the TF representations accurately for a time-varying signal. Due to this problem, high-resolution techniques are involved in the development of TFA techniques. Thus, these high-resolution techniques retain the ability to reconstruct the original time series signal. Thus, the time-varying features can be determined easily and the multicomponent modes can be decomposed effectively. The development goal of the TFA techniques is Ideal TFA (ITFA) and expressed as in equation (1).

$$\mathrm{ITFA}(t,\omega) = \sum_{k=1}^{K} A_k(t)\delta\left(\omega - \varphi_k'(t)\right)e^{i\varphi_k(t)}, \tag{1}$$

where $\delta()$ represents the Dirac delta function and degenerates to Kronecker delta function while processing discrete signal. Expression (1) depends on the multicomponent nonstationary signal model and expressed as in equation (2).

$$s(t) = \sum_{k=1}^{K} s_k(t) = \sum_{k=1}^{K} A_k(t)e^{i\varphi_k(t)}, \tag{2}$$

where $A_k(t)$ represents the instantaneous amplitude (IA), $\varphi_k(t)$ represents the instantaneous phase (IP), and its first-order derivative $\varphi'_k(t)$ represents the instantaneous frequency (IF). From expression (1), the ITFA representation has high concentrated energy and present in the IF trajectories only. Unfortunately, there are certain drawbacks in conventional TFA techniques limiting their applications in real-world data processing. To overcome the drawbacks, new techniques such as reassignment method (RM) and Synchro Squeezing Transform (SST) are introduced. The RM technique enhances the readability of the true representation of TF. RM computes the newly reassigned positions for every TF point based on TF phase information. SST enhances the resolution of time-frequency signal and reconstructs the time-frequency signal. However, the SST cannot provide an exact TF representation because, the frequency reassignment operator present in the SST cannot yield an unbiased estimation for the original time-varying IF.

In order to enhance the SST's energy concentration, an iterative technique is presented that describes the strong time-varying signals and simultaneously allows for reconstructing the signal. To perform this technique, the short-time Fourier transform (STFT) operation must be performed only once. The STFT operation does not require additional parameters for demodulating the FM modes.

The STFT of a function $s \in L^2$ (R) corresponding to the real and even window $g \in L^2$ (R) is defined as expressed in equation (3).

$$G(t,\omega) = \int_{-\infty}^{+\infty} g(u-t)s(u)e^{-i\omega(u-t)}du, \tag{3}$$

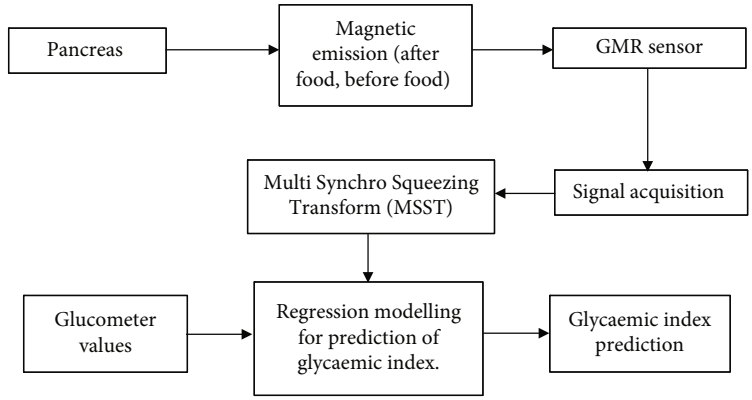

Figure 1: Detection of insulin secretion in the pancreas using the GMR sensor.

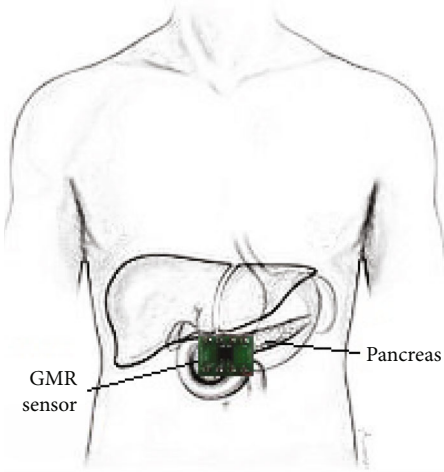

Figure 2: GMR Sensor Placed on Pancreas.

where the window $g(u)$ exists in $[-\Delta_t, \Delta_t]$. The mono-component signal model is considered first and expressed as in equation (4).

$$s(t) = A(t)e^{i\varphi(t)}. \tag{4}$$

The SST uses a frequency reassignment operator to obtain the TF coefficients and expressed as in equation (5).

$$s(u) = A(t)e^{i\left(\varphi(t)+\varphi'(t)(u-t)\right)}. \tag{5}$$

Using the SST operation, the STFT result's unclear energy is concentrated in a compact region around each mode's IF trajectories. Each mode is reconstructed by the coefficients of TF around for their IF trajectories as expressed in equation (6).

$$s_k(t) \approx (2\pi g(0))^{-1} \int_{\left|\omega-\varphi_k'(t)\right|<ds} Ts(t,\omega)d\omega. \tag{6}$$

Therefore, the SST enhances the energy concentration of TF and retains the ability to reconstruct the signal.

Additionally, the SST's representation cross-terms are considered while describing multicomponent signals. A signal having two modes is initially modeled as expressed in equation (7).

$$s(t) = s_1(t) + s_2(t) = A_1(t)e^{i\varphi_1(t)} + A_2(t)e^{i\varphi_2(t)}. \tag{7}$$

To yield an exact TF representation, the SST requires an assumption that the signal analyzed should be weak time varying. Although SST is not effective while dealing with the time-varying signals and a single SST operation can yield an exact TF representation than the STFT, another SST to an SST result acquired already can yield best TF representation. Thus, multiple SST operations are performed iteratively and thus called as Multi Synchro Squeezing Transform (MSST) and given as in equation (8).

$$\begin{aligned} Ts^{[2]}(t,\eta) &= \int_{-\infty}^{+\infty} Ts^{[1]}(t,\omega)\delta(\eta-\widehat{\omega}(t,\omega))d\omega, \\ Ts^{[3]}(t,\eta) &= \int_{-\infty}^{+\infty} Ts^{[2]}(t,\omega)\delta(\eta-\widehat{\omega}(t,\omega))d\omega, \\ &\vdots \\ Ts^{[N]}(t,\eta) &= \int_{-\infty}^{+\infty} Ts^{[N-1]}(t,\omega)\delta(\eta-\widehat{\omega}(t,\omega))d\omega. \end{aligned} \tag{8}$$

Finally, the processed biomagnetic signal of pancreas from the MSST and glucometer correlation are performed for validation.

4. Results and Discussion

The insulin secretion from pancreas is detected via biomagnetic signals acquired from pancreas of diabetic person. The GMR sensor is adhesively placed over the surface of pancreas region. The biomagnetic signals are acquired from pancreas before meal intake and after meal intake. The pancreas biomagnetic signal MSST analysis shows the influence of insulin on pancreas biomagnetic signal.

4.1. Case 1: Pancreas Biomagnetic Signal before Meal Intake—MSST Analysis. The logarithm of the MSST analysis

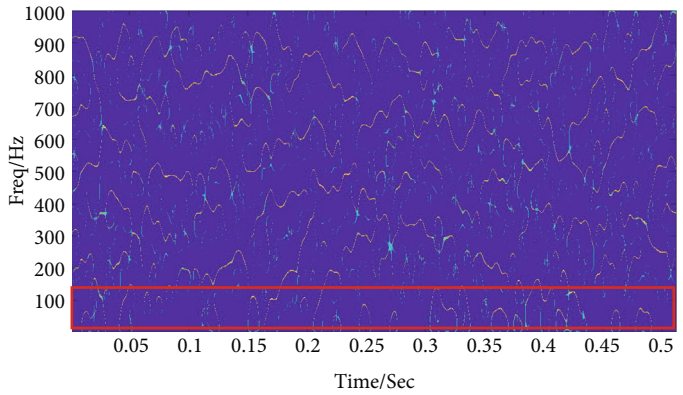

Figure 3: Logarithm of the MSST analysis result (before meals).

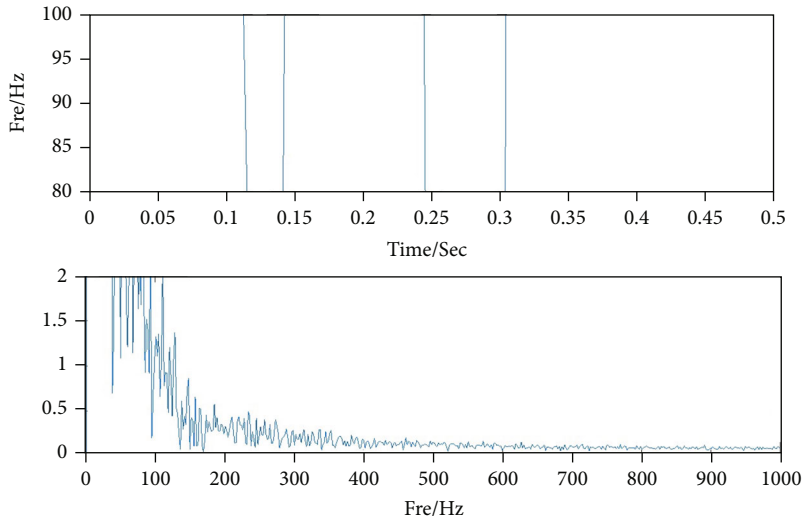

Figure 4: Detected IF trajectory of mode M1 and its spectrum (before meals).

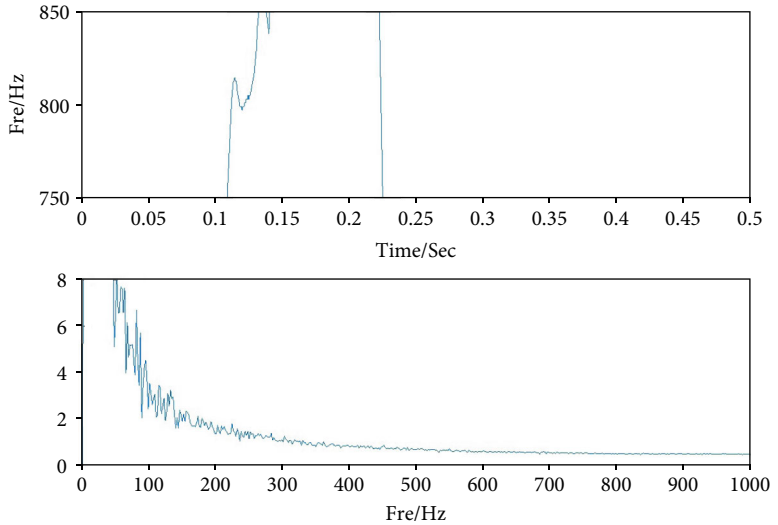

Figure 5: Detected IF trajectory of mode M2 and its spectrum (before meals).

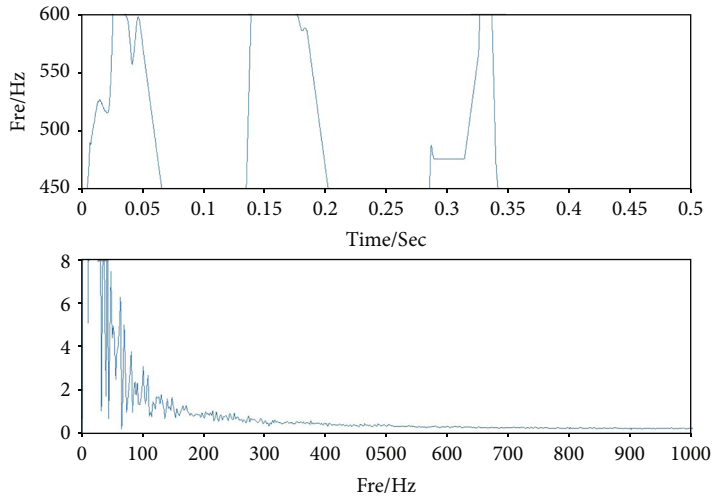

Figure 6: Detected IF trajectory of mode M3 and its spectrum (before meals).

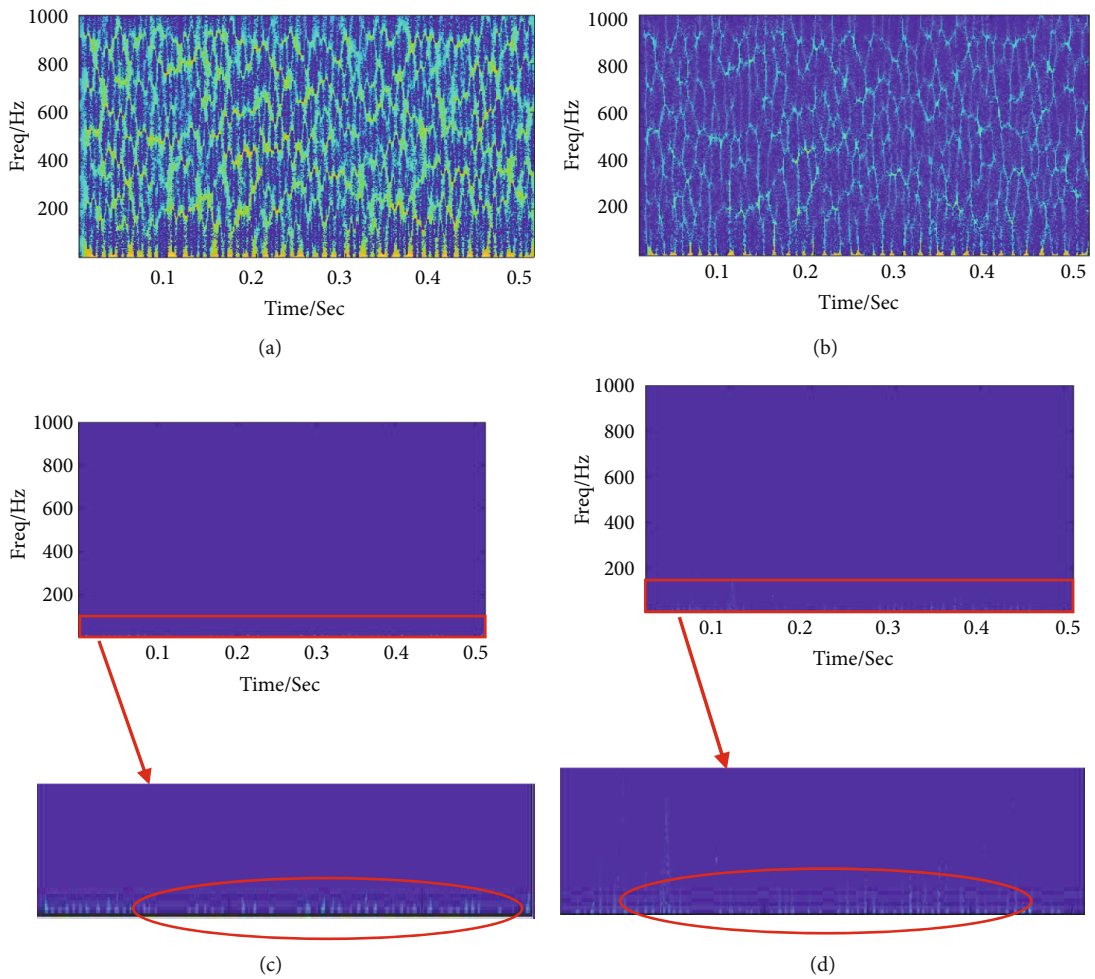

Figure 7: Logarithm of (a) SST result, (b) RM result, (c) second-order SST result, and (d) fourth-order SST result (before meals).

of pancreas biomagnetic signal before food intake is shown in Figure 3. The biomagnetic signal analyzes for the three modes M1, M2, and M3 of MSST. The three modes and their TF features are characterized to represent the features of the biomagnetic signal emitted from the pancreas before meal consumption.

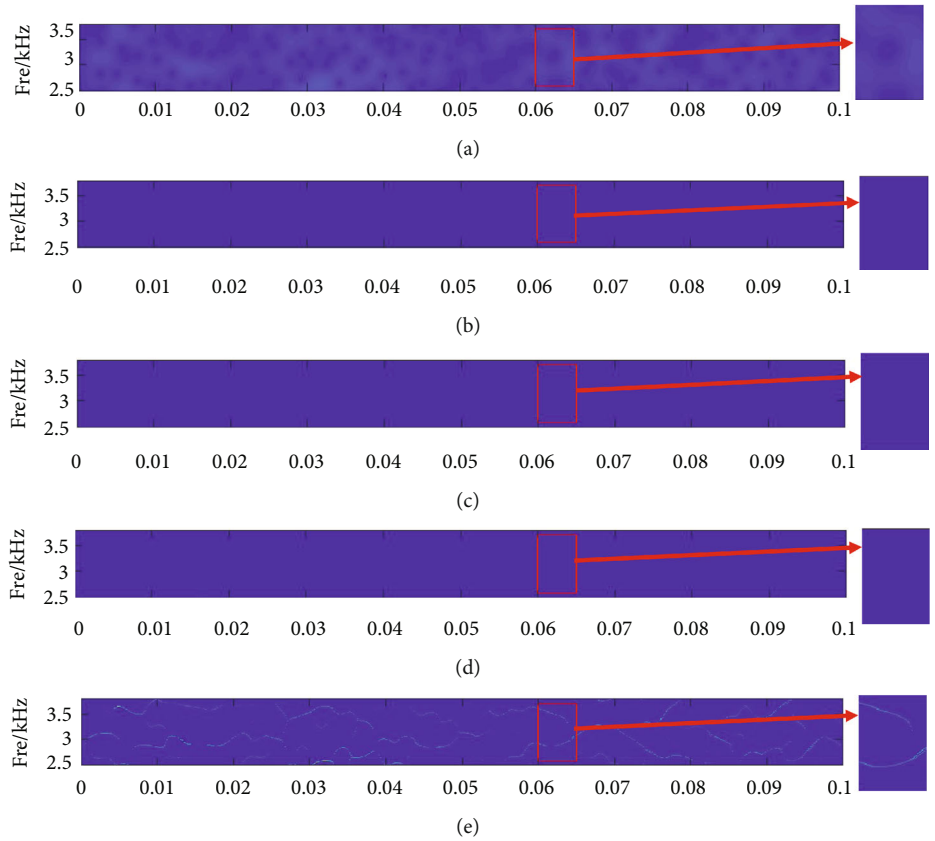

Figure 8: (a) STFT result, (b) SST result, (c) second-order SST result, (d) fourth-order SST result, and (e) MSST result (before meals).

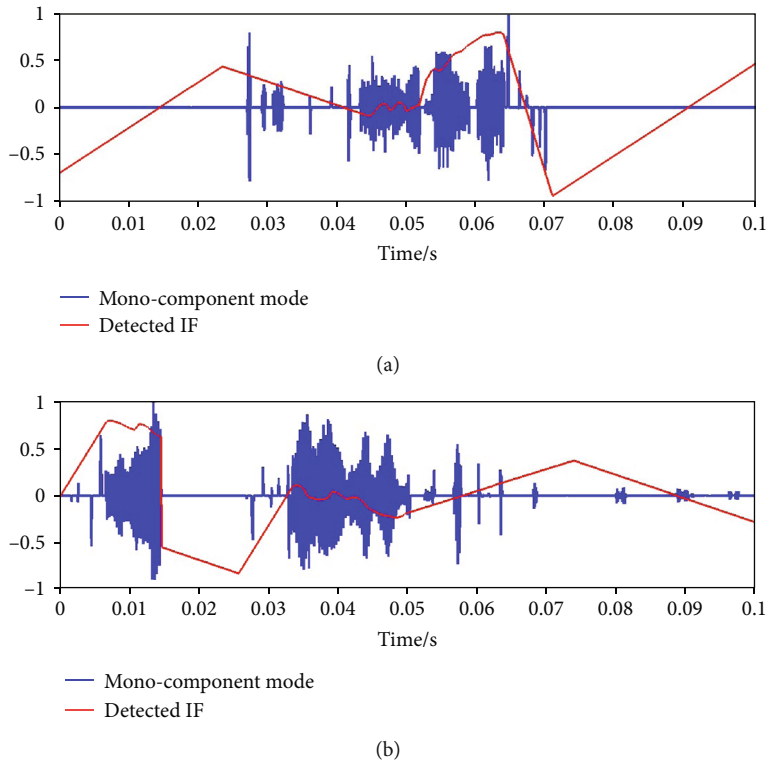

Figure 9: (a) Waveform of mode 1 and its IF (b) waveform of mode 2 and its IF (before meals).

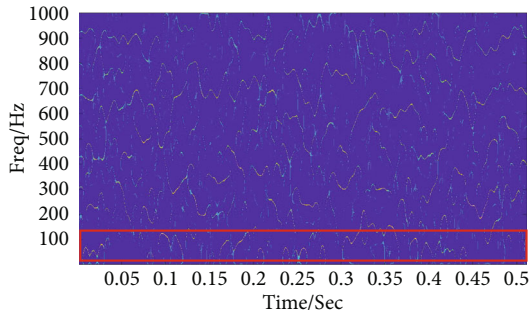

Figure 10: Logarithm of the MSST analysis result (after meals).

Figure 4 represents the IF of the mode M1 before meals. The IF of mode M1 has strong amplitude since the MSST slices time frequency (TF) of different modes with narrow frequency band, TF energy, and larger components at frequencies 40 Hz, 99 Hz, and 101 Hz, respectively. The signal slicing increases temporal resolution of pancreatic biomagnetic signal and exposes nonlinear signal variations.

Figure 5 represents the IF of mode M2 before meals. The IF of mode M2 has weak amplitude and larger components at frequencies 50 Hz, 70 Hz, and 80 Hz, respectively. However, the temporal resolution of pancreatic biomagnetic signal is reduced due to higher estimate of instantaneous frequency by STFT.

Figure 6 represents the IF of mode M3 before meals. The IF of mode M3 has weak amplitude and larger components at frequencies 50 Hz, 70 Hz, and 80 Hz, respectively.

Figure 7 represents the logarithmic analysis of SST result, RM result, second-order SST result, and fourth-order SST result before meals. The TF results are unclear since the traditional SST-based techniques cannot yield enough distance to reassign the unclear TF coefficients to the original IF region.

To interpret more detailed information on the features of the biomagnetic signal emitted from pancreas before meals, the key focus is on the features of TF around 2500 Hz-4000 Hz. The TF representations created by STFT, SST, second-order SST, fourth-order SST, and MSST before meals are shown in Figure 8, and the local features are shown in the right side. Figure 8(a) represents that the STFT characterizes the frequency band and duration time roughly of each signal component. Due to Heisenberg's uncertainty principle, the STFT result's TF energy blurs heavily. Figures 8(b)–8(d) represent that the SST cannot yield concentrated result. Figure 8(e) represents that the MSST technique yields more concentrated result. The MSST result represents that there must be two mono-component modes in the frequency bands 2500 Hz-4000 Hz.

Based on the results of MSST, two IF modes are identified. Additionally, these two modes' detailed features can be understood by the waveform plot of two modes along with their IF trajectories before meals as shown in Figure 9.

4.2. Case 2: Pancreas Biomagnetic Signal after Food Intake—MSST Analysis. The logarithm of the MSST analysis result of the signal for three modes M1, M2, and M3 taken after meals is shown in Figure 10. The three modes and their TF features are characterized to show the minimal variations of pancreas magnetic signal. The TF features of pancreas magnetic signal enhance by viewing the logarithm of acquired pancreas signal. The logarithmic analysis of acquired pancreas signal shows the change in magnetism due to insulin secretion.

Then ridge detection algorithm is utilized to determine the IF of three modes. Figure 11 represents the IF of the mode M1 after meals. The IF of mode M1 has strong amplitude and larger components at frequencies 60 Hz, 100 Hz, 130 Hz, 160 Hz, and 170 Hz, respectively.

Figure 12 represents the IF of mode M2 after meals. The IF of mode M2 has weak amplitude and larger components at frequencies 30 Hz, 50 Hz, and 70 Hz, respectively.

Figure 13 represents the IF of mode M3 after meals. The IF of mode M3 has weak amplitude and larger components at frequencies 50 Hz, 70 Hz, and 80 Hz, respectively.

Figure 14 represents the logarithmic analysis of SST result, RM result, second-order SST result, and fourth-order SST result after meals. The figure represents that the TF results have slight change in the TF representations.

To understand more details from the information on the features of the biomagnetic signal after meals, the key focus is on the features of TF around 2500 Hz-4000 Hz. The TF representations created by STFT, SST, second-order SST, fourth-order SST, and MSST after meals are shown in Figure 15, and the local features are shown in the right side. Figure 15(a) represents that the STFT characterizes the frequency band and duration time accurately of each signal component. The SST does not yield concentrated result for biomagnetic signal emitted from pancreas as in Figures 15(b)–15(d). Figure 15(e) represents the MSST technique which yields more concentrated result. The MSST result shows three trajectories which show the mono-component modes in the frequency bands 2.5 kHz–3.5 kHz.

Based on the results of MSST, two IF modes are identified. Additionally, these two modes' detailed features can be understood by the waveform plot of two modes along with their IF trajectories for the pancreas biomagnetic signal emission after meal consumption. The magnetic emission from the pancreas due to meal consumption undergoes amplitude modulation and frequency oscillations. The biomagnetic signal has transient amplitude-modulated signal and frequency-modulated law components as shown in Figure 16. Figures 16(a) and 16(b) show instantaneous frequency estimation of the pancreas biomagnetic signal for modes M1 and M2, respectively.

The pancreas biomagnetic signal's statistical parameters are shown in Table 1. The glycaemic index predicts from kurtosis value of the pancreas biomagnetic signal via regression modelling.

4.3. Regression Modelling. The general form of regression modelling is given by

$$y = \mathrm{m}x + c, \tag{9}$$

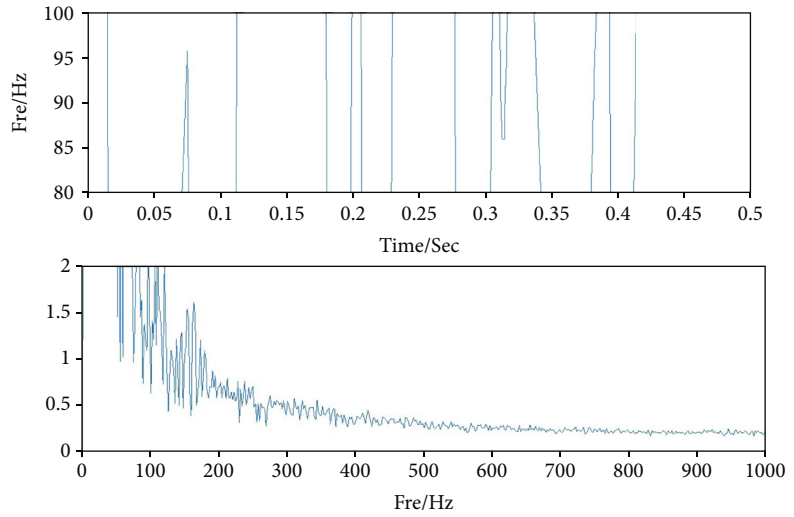

Figure 11: Detected IF trajectory of mode M1 and its spectrum (after meals).

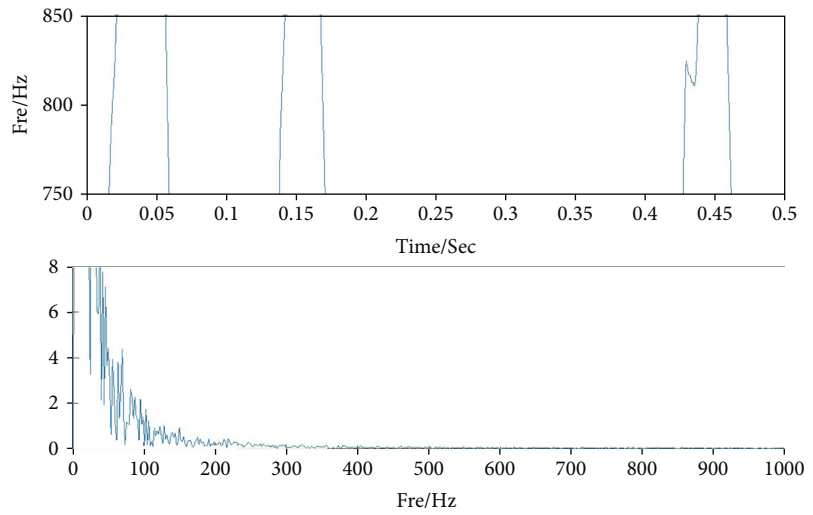

Figure 12: Detected IF trajectory of mode M2 and its spectrum (after meals).

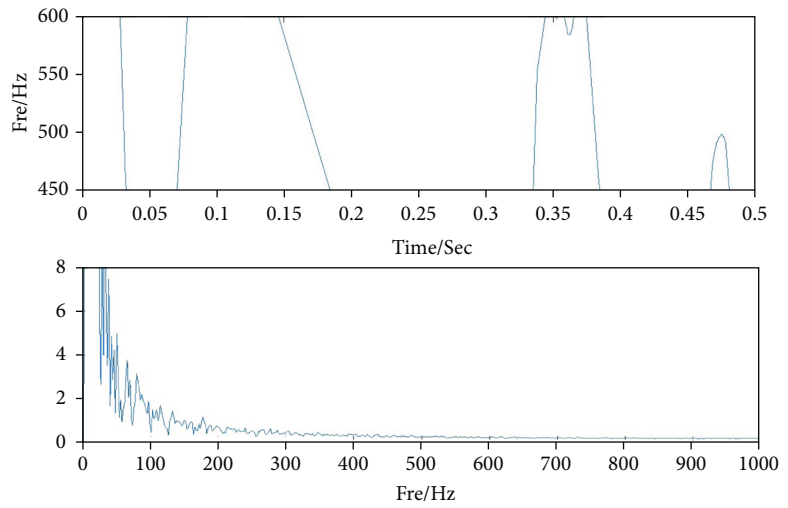

Figure 13: Detected IF trajectory of mode M3 and its spectrum (after meals).

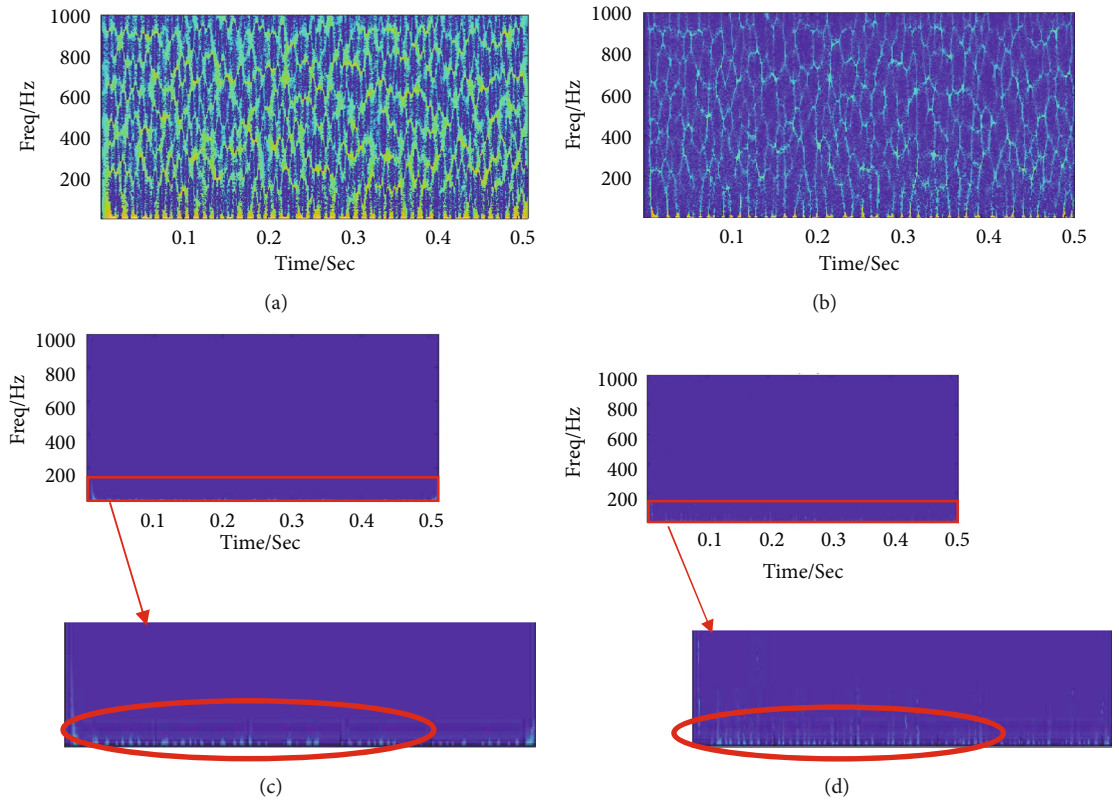

Figure 14: Logarithm of (a) SST result, (b) RM result, (c) second-order SST result, and (d) fourth-order SST result (after meals).

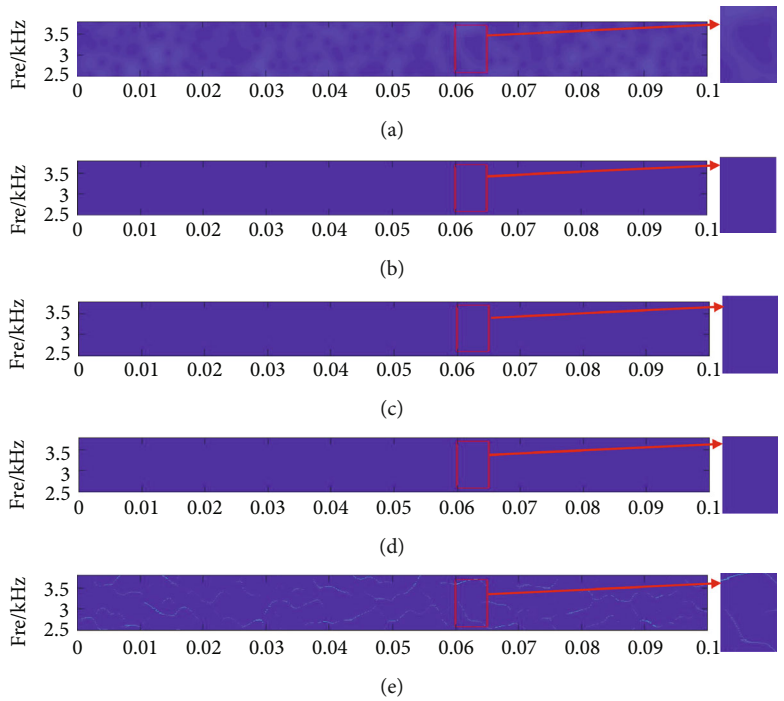

Figure 15: (a) STFT result, (b) SST result, (c) second-order SST result, (d) fourth-order SST result, and (e) MSST result (after meals).

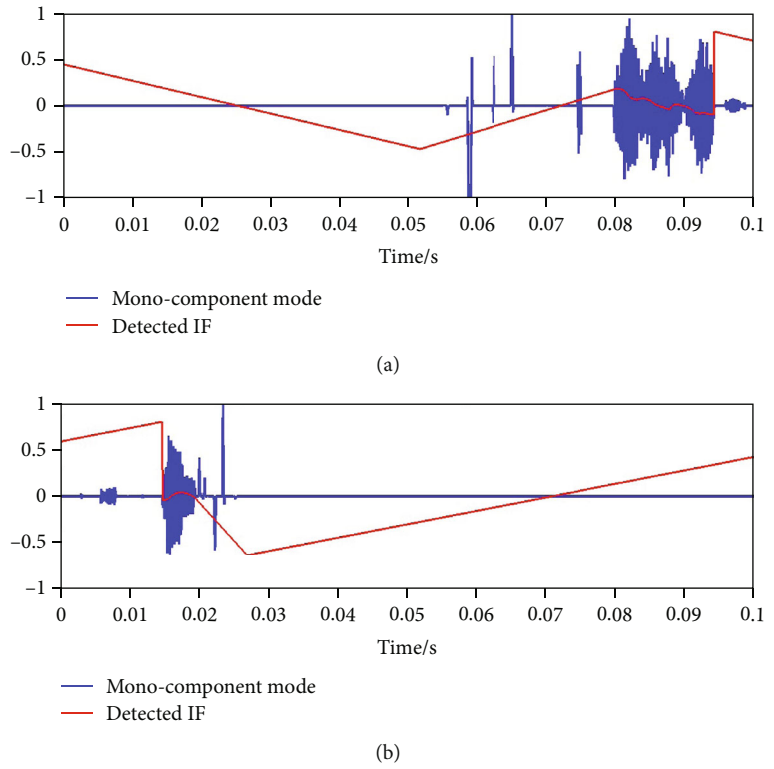

Figure 16: (a) Waveform of mode 1 and its IF (b) waveform of mode 2 and its IF (after meals).

Table 1: Pancreas biomagnetic signal statistical parameters.

Pancreas biomagnetic signal (diabetic person)	Mean (signal)	Standard deviation (signal)	Kurtosis (signal)	Glucometer value (laboratory instrument)	Predicted value
Before meal consumption	0.21589	1.259	0.95482	85	89
After meal consumption	0.38518	1.3584	0.9127	122	122.00

where "y" represents the response variable and "x" represents the predictor variable.

The glycaemic index predictor equation is given by

$$\hat{y} = -783.47578X + 837.07835. \quad (10)$$

The predictor equation was obtained based on kurtosis values from signals obtained from fifty diabetic patients.

5. Conclusion

The study concludes change in magnetic signal emission from the pancreas due to meal consumption. The GMR sensor is placed over the pancreas region to detect magnetic emission. The GMR acquired magnetic signal was processed with MSST to estimate instantaneous frequency change and visualize amplitude modulation and frequency oscillations. The amplitude modulation and frequency oscillations provide a noninvasive way to detect the pancreas insulin secretion activity. Experimental results show the proposed method analyses magnetic emission from the pancreas effectively for before and after meal consumption cases. The magnetic emission from the pancreas varies proportional to the type of food intake. Furthermore, magnetic signal emission from the pancreas can be used to estimate insulin intake for diabetic person.

Data Availability

No data were used to support this study.

Ethical Approval

All procedures were in accordance with the 1964 Helsinki Declaration (and its amendments). No approval by ethical committee or institutional review board was required.

Conflicts of Interest

The authors declare no conflict of interest.

References

[1] X. Huang, S. Li, J. Schultz, Q. Wang, and Q. Lin, "A capacitive MEMS viscometric sensor for affinity detection of glucose," *Journal of Microelectromechanical Systems*, vol. 18, no. 6, pp. 1246–1254, 2009.

[2] B. Lewis, *Development of the Pancreas and Related Structures*, Wiley Blackwell, 2018.

[3] A. J. Bandodkar, S. Imani, R. Nuñez-Flores et al., "Re-usable electrochemical glucose sensors integrated into a smartphone platform," *Biosensors & Bioelectronics*, vol. 101, no. 1, pp. 181–187, 2018.

[4] A. Facchinetti, G. Sparacino, and C. Cobelli, "Online denoising method to handle intraindividual variability of signal-to-noise ratio in continuous glucose monitoring," *IEEE Transactions on Biomedical Engineering*, vol. 58, no. 9, pp. 2664–2671, 2011.

[5] V. P. Rachim and W.-Y. Chung, "Wearable-band type visible-near infrared optical biosensor for non-invasive blood glucose monitoring," *Sensors and Actuators B: Chemical*, vol. 286, no. 2018, pp. 173–180, 2019.

[6] A. Hennig, J. Lauko, A. Grabmaier, and C. Wilson, "Wireless tear glucose sensor," *Procedia Engineering*, vol. 87, no. 40, pp. 66–69, 2014.

[7] P. G. Jacobs, J. el Youssef, J. Castle et al., "Automated control of an adaptive Bihormonal, dual-sensor artificial pancreas and evaluation during inpatient studies," *IEEE Transactions on Biomedical Engineering*, vol. 61, no. 10, pp. 2569–2581, 2014.

[8] H. M. Saraoglu, A. O. Selvi, M. A. Ebeoglu, and C. Tasaltin, "Electronic nose system based on quartz crystal microbalance sensor for blood glucose and HbA1c levels from exhaled breath odor," *IEEE Sensors Journal*, vol. 13, no. 11, pp. 4229–4235, 2013.

[9] G. Sparacino, F. Zanderigo, S. Corazza, A. Maran, A. Facchinetti, and C. Cobelli, "Glucose concentration can be predicted ahead in time from continuous glucose monitoring sensor time-series," *IEEE Transactions on Biomedical Engineering*, vol. 54, no. 5, pp. 931–937, 2007.

[10] Z. Wang, C. Wang, and P. Lathan, "Breath acetone analysis of diabetic dogs using a cavity Ringdown breath analyzer," *IEEE Sensors Journal*, vol. 14, no. 4, pp. 1117–1123, 2014.

[11] A. Sedighi, M. Montazer, and S. Mazinani, "Synthesis of wearable and flexible NiP0.1-SnOx/PANI/CuO/cotton towards a non-enzymatic glucose sensor," *Biosensors & Bioelectronics*, vol. 135, no. 1, pp. 192–199, 2019.

[12] X. Xuan, H. S. Yoon, and J. Y. Park, "A wearable electrochemical glucose sensor based on simple and low-cost fabrication supported micro-patterned reduced graphene oxide nanocomposite electrode on flexible substrate," *Biosensors & Bioelectronics*, vol. 109, no. 1, pp. 75–82, 2018.

[13] Y. Wang, X. Wang, W. Lu, Q. Yuan, Y. Zheng, and B. Yao, "A thin film polyethylene terephthalate (PET) electrochemical sensor for detection of glucose in sweat," *Talanta*, vol. 198, no. 1, pp. 86–92, 2019.

[14] Y. Zhang, Y. Wang, J. Jia, and J. Wang, "Nonenzymatic glucose sensor based on graphene oxide and electrospun NiO nanofibers," *Sensors and Actuators B: Chemical*, vol. 171-172, no. 1, pp. 580–587, 2012.

[15] N.-Y. Kang, A. A. P. Soetedjo, N. S. Amirruddin, Y. T. Chang, O. Eriksson, and A. K. K. Teo, "Tools for bioimaging pancreatic β cells in diabetes," *Trends in Molecular Medicine*, vol. 25, no. 8, pp. 708–722, 2019.

[16] C. Guay, J. K. Kruit, S. Rome et al., "Lymphocyte-derived exosomal microRNAs promote pancreatic β cell death and may contribute to type 1 diabetes development," *Cell Metabolism*, vol. 29, no. 2, pp. 348–361.e6, 2019.

[17] E. Ganesh, N. R. Shanker, and M. Priya, "Non-invasive measurement of glaucoma disease at earlier stage through GMR sensor AH biomagnetic signal from eye and RADWT algorithm," *IEEE Sensors Journal*, vol. 19, no. 14, pp. 5404–5412, 2019.